Clim Dyn
DOI 10.1007/s00382-009-0693-6

Forced response of the East Asian summer rainfall over the past millennium: results from a coupled model simulation

Jian Liu · Bin Wang · Hongli Wang · Xueyuan Kuang · Ruyuan Ti

Received: 20 May 2009 / Accepted: 16 October 2009

Abstract The centennial–millennial variation of the East Asian summer monsoon (EASM) precipitation over the past 1000 years was investigated through the analysis of a millennium simulation of the coupled ECHO-G model. The model results indicate that the centennial–millennial variation of the EASM is essentially a forced response to the external radiative forcing (insolation, volcanic aerosol, and green house gases). The strength of the response depends on latitude; and the spatial structure of the centennial–millennial variation differs from the interannual variability that arises primarily from the internal feedback processes within the climate system. On millennial time scale, the extratropical and subtropical precipitation was generally strong during Medieval Warm Period (MWP) and weak during Little Ice Age (LIA). The tropical rainfall is insensitive to the effective solar radiation forcing (insolation plus radiative effect of volcanic aerosols) but significantly responds to the modern anthropogenic radiative forcing. On centennial time scale, the variation of the extratropical and subtropical rainfall also tends to follow the effective solar radiation forcing closely. The forced response features in-phase rainfall variability between the extratropics and subtropics, which is in contrast to the anti-correlation on the interannual time scale. Further, the behavior of the interannual–decadal variation in the extratropics is effectively modulated by change of the mean states on the millennial time scale, suggesting that the structure of the internal mode may vary with significant changes in the external forcing. These findings imply that on the millennial time scale, (a) the proxy data in the extratropical EA may more sensitively reflect the EASM rainfall variations, and (b) the Meiyu and the northern China rainfall provide a consistent measure for the EASM strength.

Keywords East Asian summer monsoon · Millennial time scale · External forcing · Coupled climate model

1 Introduction

The EASM has the largest meridional extent (roughly from 5°N to 55°N) among all the regional monsoons on globe. Accordingly, both the climatology and interannual variations of the EASM have complex spatial structures, which involve three circulation systems, the tropical western North Pacific monsoon trough or intertropical convergence zone (ITCZ), the subtropical western Pacific high and subtropical frontal rain band (the Maiyu front), and the extratropical baroclinic disturbances (e.g., Tao and Chen 1987; Chang et al. 2000b). The large meridional extent of the EASM involves rich interactive processes between the tropics and midlatitude, which has attracted much attention in the monsoon study. Due to its large latitudinal extent, the EASM provides a unique opportunity for understanding of

J. Liu (✉) · H. Wang · R. Ti
State Key Laboratory of Lake Science and Environment, Nanjing Institute of Geography and Limnology, Chinese Academy of Sciences, 73 East Beijing Road, 210008 Nanjing, China
e-mail: jianliu@niglas.ac.cn

B. Wang
Department of Meteorology and IPRC, University of Hawaii at Manoa, Honolulu, HI 96822, USA

X. Kuang
School of Atmospheric Sciences, Nanjing University, 210093 Nanjing, China

Published online: 10 November 2009

the latitudinal differences of the monsoon response to external forcing and internal feedback processes.

The modern meteorologists have focused on the interannual variability of the EASM, which arises primarily from the impacts of El Nino-Southern Oscillation (ENSO) (Guo 1983; Fu 1987; Ju and Slingo 1995; Chang et al. 2000a) and local monsoon–ocean–land interaction (e.g., Wang et al. 2000; Wang and Zhang 2002; Lau and Nath 2000, 2006). In contrast to our advanced knowledge of the interannual variation of the EASM, the behavior of its variation on the centennial–millennial time scale is little known.

There are a number of controversial issues in understanding the EASM variability between the modern and paleo-monsoon scientists. On the interannual time scale, when southerly monsoon penetrates deeply into the northern China, the extratropical EA has plentiful rainfall, but the subtropical rainfall (known as Meiyu, the "plum rain", in Chinese and Baiu in Japanese) tends to be suppressed (Ding 1992). With this "modern" definition, a strong EASM means a deficient Meiyu or Biau. In paleo-monsoon community, however, the strength of the EASM is often measured by the stalagmite proxy data obtained from Hulu (meaning "bottle gourd" in Chinese) cave (Wang et al. 2005), which is located in the subtropical Meiyu region and thus a strong EASM means an abundant Meiyu. Further, in paleo-monsoon community, an enhanced EASM is often considered as a result of the northward advance or enhancement of the ITCZ (e.g., Yancheva et al. 2007). This perception assumes an in-phase variation of ITCZ and EA subtropical monsoon (Meiyu). On the other hand, the modern meteorologists have found that the interannual–decadal variations of Meiyu tend to be out of phase with the tropical (or ITCZ) rainfall (Nitta 1987; Huang and Wu 1989).

These conflict concepts have been a major roadblock for the communication between the modern and paleo-monsoon scientists. Why do the two communities have contradictory perspectives? Wang et al. (2008) and Liu et al. (2008) pointed out that the interannual variation is primarily due to internal feedback processes within the coupled climate system such as ENSO-monsoon connection, whereas the monsoon variability on orbital time scales arises primarily from various forcings that are external to the coupled climate system. For convenience, in the present study the former will be referred to as internal mode of variability while the latter is called forced mode of variability. It has been postulated that the mechanisms that govern the internal modes may fundamentally differ from those that govern the external mode, thereby the temporal–spatial structures of the forced and internal modes could be different, which may explain the different perspectives between the modern and paleo monsoon communities (Wang et al. 2008; Liu et al. 2008). This hypothesis is important for understanding the behavior of the internal mode and forced mode of the monsoon variability. However, it has not been tested. One of the objectives of this study is to elaborate the differences and linkages between the forced and internal mode of variability.

To fulfill this objective, the coupled climate models' long-term simulations over the past millennium may provide an excellent opportunity of research. Over the past millennium, the effective solar radiation forcing has experienced appreciable millennium and centennial variations. The term "effective solar radiation forcing" in this paper means the sum of the solar radiation and the radiative effect of the volcanic aerosols. The effective solar radiation flux between the Medieval Warm Period (MWP) and Little Ice Age (LIA) differs by about 1.87 W/m^2 in the coupled model simulation (Table 1). In the presence of external radiative forcing, it is not clear whether the extratropical and subtropical rainfalls vary in tandem or not. It is also unknown whether ITCZ is in phase or out-of-phase with subtropical EA rainfall. Yet, this knowledge is crucial for adequate interpretation of variety of proxy data obtained in different regions of the EASM domain.

The present study aims at addressing these issues by analysis of the coupled climate model's millennial simulation. In the next section, we will first introduce the coupled model and evaluate its performance. Since the EASM

Table 1 Comparison of the simulated (in the ERIK forced run) and the observed (CMAP) MJJA mean precipitation rate (mm/day) for extratropical (36°N–50°N, 100°E–120°E), subtropical (21°N–35°N, 100°E–120°E), and tropical (6°N–20°N, 100°E–120°E) EA regions and the effective solar radiation forcing (W/m^2) during the medieval warm period (MWP), little ice age (LIA) and present-day warm period (PWP)

MJJA mean precipitation (mm/day)	MWP (1100–1200)	LIA (1600–1700)	PWP (1920–1990)	CMAP (1979–2007)
36°N–50°N, 100°E–120°E	**2.12***	**1.98**	2.07	1.71
21°N–35°N, 100°E–120°E	**5.13**	**4.99**	5.07	5.76
6°N–20°N, 100°E–120°E	7.74	**7.79**	**8.01**	8.93
Effective solar radiation (W/m^2)	1365.94	1364.07	1366.82	

* The *bold numbers* represent the changes between MWP and LIA or between the LIA and PWP are statistically significant at 95% confidence level

has large meridional extent including tropics, subtropics and midlatitude, in Sect. 3 we focus on the latitudinal dependence of the millennial and centennial monsoon variation. To address the issues being raised earlier in this section, we examine, in Sect. 4, the meridional structures of the forced mode of EASM in comparison with those of the internal mode. Sect. 5 studies the possible modulation of the millennial variation on the behavior of the inter-annual variations. The last section offers a summary and discusses ramifications of the results on interpretation of EASM variability.

2 Validation of the model performance

The coupled model used in this study is the ECHO-G model, which consists of the spectral atmospheric model ECHAM4 and the global ocean circulation model HOPE-G, both of which were implemented and developed at the Max-Planck Institute for Meteorology (MPI) in Hamburg (Legutke and Voss 1999). ECHAM4 is the fourth generation of atmospheric general circulation model, which is based on primitive equations with a mixed p–σ coordinate system (Roeckner et al. 1996). The horizontal resolution of the model is T30, or approximately 3.75° × 3.75°, and the vertical resolution is 19 levels with five upper levels being located above 200 hPa. The time-step of integration is 24 min. The horizontal resolution of the ocean model HOPE-G is about 2.8° × 2.8° with a grid refinement in the tropical regions, where the meridional grid point separation reaches 0.5°. The ocean model has 20 vertical levels (Wolff et al. 1997). The ECHAM4 and HOPE-G are coupled through the coupler OASIS3.

The model output analyzed was obtained from the millennium integrations of the coupled ECHO-G model. The millennial integrations for the period 1000–1990 AD include a free (control) run (Zorita et al. 2003), which was generated using fixed external (annually cycle) forcing that is set to the present-day values, and a forced run (called ERIK) (Zorita et al. 2005), which was forced by three external forcing factors: solar variability, greenhouse gases concentrations in the atmosphere including CO_2 and CH_4, and an estimated radiative effect of stratospheric volcanic aerosols. The radiation flux at the top of the atmosphere is calculated with the effects of sunspots and cosmic ray isotope included (Crowley 2000). The radiation forcing effect of volcanic ash is first estimated by the concentration of sulfides in the Greenland ice core and then calculated by the atmospheric model (Robock and Free 1996). The concentration of CO_2 (Etheridge et al. 1996) and CH_4 (Blunier et al. 1995) are both obtained from the ice core data in Antarctic. The time sequences of these forcings are shown in Fig. 1. The term effective solar radiation is used through the context to represent the sum of the solar constant and the effects of volcanic aerosols.

The data used for validation of the model performance on the present day climate include: (1) the precipitation dataset covering both land and ocean for the period of 1979–2006 compiled by Climate prediction center Merged Analysis of Precipitation (CMAP) (Xie and Arkin 1995), and (2) the National Centers for Environmental Prediction (NCEP)-Department of Energy (DOE) reanalysis 2 data (NCEP2) (Kanamitsu et al. 2002). For comparison with historical records, we used reconstructed temperature proxy data in China for the past 2000 years compiled by Yang et al. (2002) and the rainfall proxy at Wanxiang cave deduced by Zhang et al. (2008).

Faithful analysis of the EASM response to external forcing should be based on rigorous verification of the model performance, especially on the annual cycle,

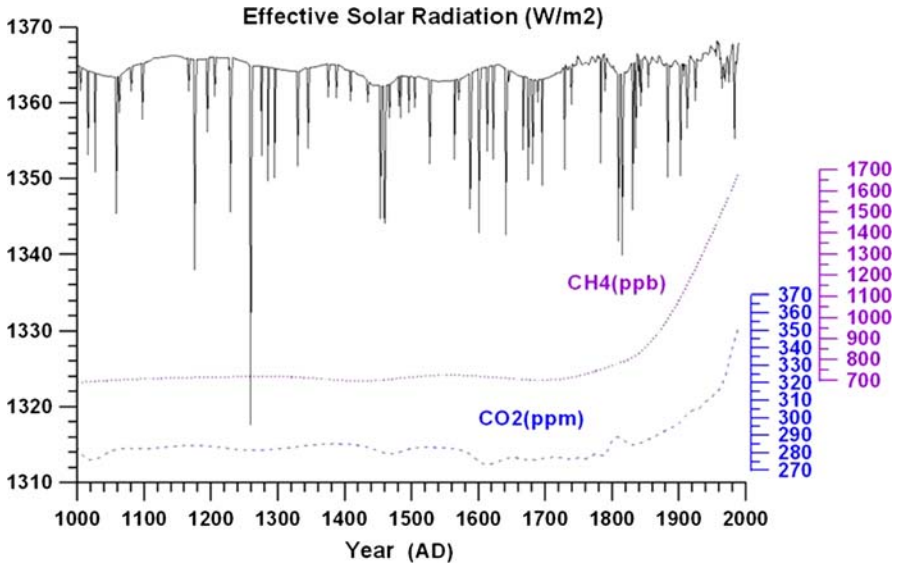

Fig. 1 The temporal variation of external forcing factors used in ECHO-G ERIK forced simulation: the effective solar radiation forcing (insolation plus volcanic aerosol effect), the concentration of CH_4 and CO_2

because the annual cycle exemplifies a forced response. The analysis of the EASM variability in a coupled climate model is in general a great challenge because the current climate models have notorious problems in realistic simulation of the monsoon annual cycle in the EA and western North Pacific sector (Kang et al. 2002; Wang et al. 2004). Evaluation of EASM also requires special consideration that takes into account the unique features of the EASM. First, in view of the large meridional extent, the EASM is divided into three sub-regions in this study: the tropics (6°N–20°N), the subtropics (21°N–35°N), and the extratropics (36°N–50°N). We will focus on the precipitation averaged over these three different latitude bands. Second, the EA is also a region where the seasonal march of the monsoon rain belt is most spectacular on Earth. The monsoon rain band moves from 15°N in May all the way to 45°N in late July. The summer rainy season starts over Indo-China peninsula in early May (Matsumoto and Murakami 2002; Ding and Sikka 2006), and over the South China Sea by mid-May (Tao and Chen 1987). The rainy season generally retreats toward the end of August except in a restricted region of the tropical EA, northwest central China, and northern Japan (Wang and LinHo 2002). Thus, May through August is considered as the primary summer rainy season over EA. In this study we take May–August (MJJA) as the summer season in EA.

Figure 2 compares the model simulated climatology in the ERIK run (1961–1990) with observation (CMAP 1979–2007). Precipitation is emphasized because it is a more rigorous test and because its variation is our primary concern. The observed annual mean precipitation generally decreases northwestward from the southeast Asian marginal seas toward the arid central continental Asia; and the contour of 3 mm/day (about 1,100 mm/year) extends from northeast India to South Korea (Fig. 2a). The ERIK run replicates this gross feature realistically. In the entire EASM domain (5°N–55°N, 100°E–140°E), the pattern correlation coefficient between observation (CMAP) and model simulation is 0.87, and the domain averaged root mean square error is 1.19 mm/day (Fig. 2b). Surprisingly, the model's performance is comparable to the corresponding NCEP-2 reanalysis climatology (Fig. 2c). While the overall features are simulated reasonably well, the rainfall is underestimated over the Bay of Bengal, South Korea, and along the Okinawa island chain, while it is overestimated over the eastern flank of the Tibetan Plateau.

Figure 3 compares the simulated and observed annual cycles of the precipitation rate in the following three subregions: the extratropical, subtropical, and tropical EA. The annual cycle in the extratropical region is well simulated with a peak rainy month in July and a minimum in January, but the spring rainfall is over-produced. Over the subtropical latitudes, the observed June peak was marginally captured but the precipitation in June–August is underestimated. In the tropical region, the mean rainfall in early summer (May–July) is well simulated but the August peak and the precipitation in August–October are underestimated. Since tropical cyclone is a major contributor to the August–October rainfall over the South China Sea, the lack of August–October rain in the tropical region may be due to the model's inability to capture the tropical cyclone activity. Overall, the model performs reasonably well in simulation of the precipitation amounts in different latitudinal regions of the eastern China between 100°E and 120°E.

In order to validate the millennium variation in the forced ERIK run, the time series of the simulated surface air temperature averaged over whole China (15°N–55°N, 70°E–140°E) was presented in Fig. 4 in comparison with the reconstructed proxy data by Yang et al. (2002). Both time series feature a prominent V-shape millennial variation. Superposed on the millennium variation is a bi-centennial variation component. We have estimated the degrees of freedom using the method proposed by Livezey and Chen (1983) and found that the correlation coefficient of 0.75 between the simulated time series and proxy data is significant at 95% confidence level, but it mainly comes from the lower (>100 years) frequency variations. The

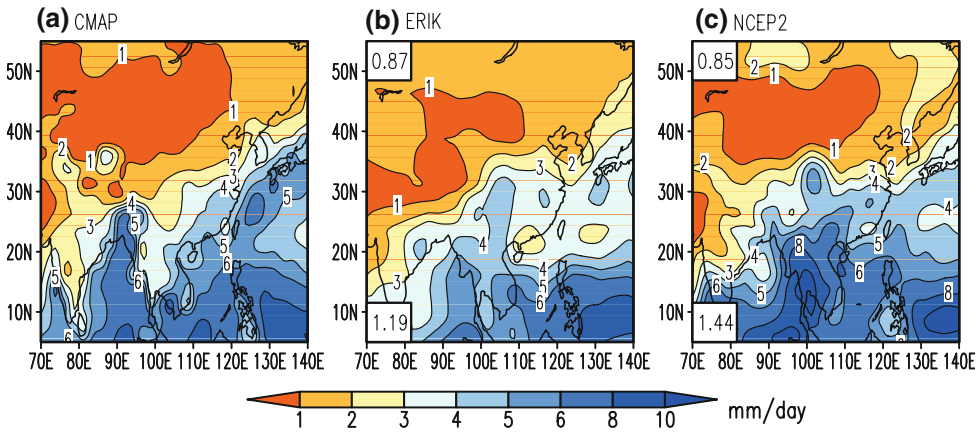

Fig. 2 Comparison of the climatological annual mean precipitation rate (mm/day) for (**a**) the observed (CMAP, 1979–2007), (**b**) ECHO-G model simulated (in the forced ERIK run, 1961–1990), and (**c**) the NCEP 2 reanalysis field (1979–2007). Pattern correlation coefficients and root mean square errors (in units of mm/day) with respect to the observation are shown in the *upper-left* (*lower-bottom*) corners of the panel **b** and **c**

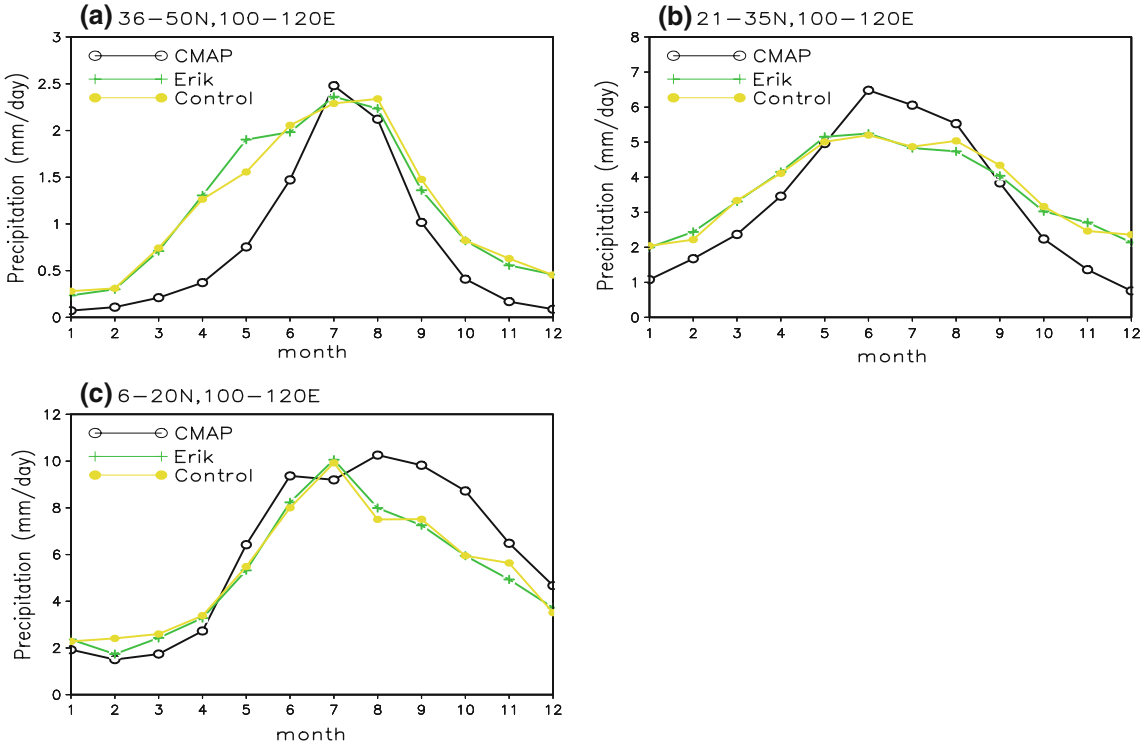

Fig. 3 Comparison of the observed (CMAP, 1979–2007) and the simulated (ECHO-G ERIK and control runs, 1961–1990) climatological annual variation of precipitation rate (mm/day) at **a** extratropical (36°N–50°N), **b** subtropical (21°N–35°N), and **c** tropical (6°N–20°N) East Asia averaged between 100°E and 120°E

correlation coefficient for the lower frequency and higher frequency (<100 years) variations are 0.87 and 0.16, respectively. The former is significant at 95% confidence level, while the latter is not. In summary, the agreement between the simulated and observed annual mean and annual cycle, as well as the centennial–millennial variation of temperature over the past 1,000 years adds confidence to our subsequent analysis of the centennial-scale precipitation variability using the same outputs from the forced (ERIK) run.

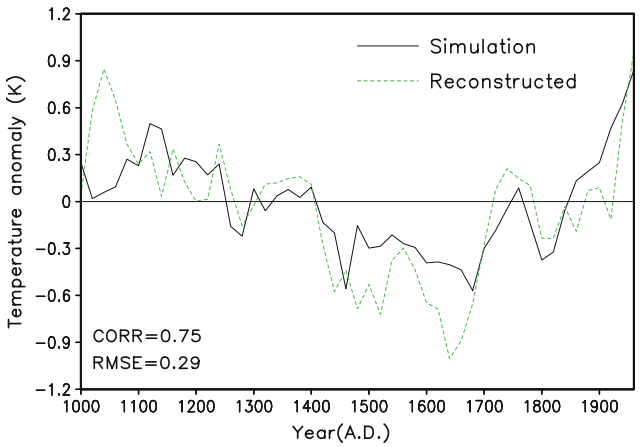

Fig. 4 Comparison of the Chinese surface air temperature variation deduced from the proxy data (Yang et al. 2002) with the simulated counterpart in the forced ERIK run. A 20-year average was applied to the time series

3 Latitude-dependent response of the EASM to the external forcing

3.1 Millennial variation

The millennial variation generally refers to variations on ~1,000 years or longer time scale and our time series is much too short to identify a full cycle of this length. Since our focus in this study is the dynamic structure and climate variation, not the periodicity, of the millennial variation, we examine the differences between the MWP and LIA, which represent two extreme phases of the latest millennial cycle. We will loosely refer to the difference between the MWP and LIA as millennium variation. Since the EASM comes across tropics, subtropics and extratropics, the first question of interest is how the EASM precipitations in the three sub-regions respond to the millennial variations in the effective solar radiation. Figure 5a–c present time series of MJJA mean precipitation rates simulated in the ERIK run for the three sub-regions. All three time series were subject to an 11-year moving average in order to underline the

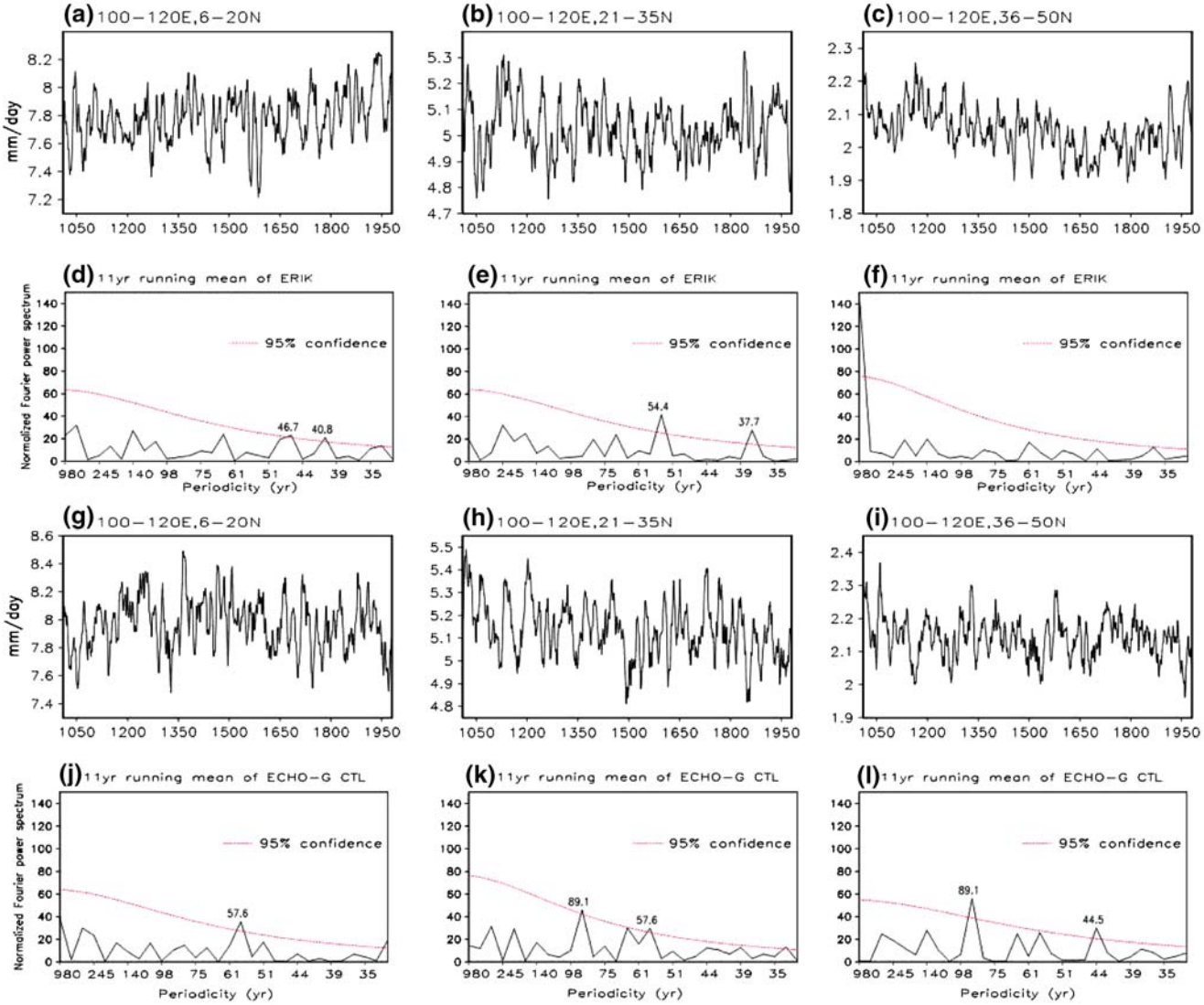

Fig. 5 The 11-year running mean time series of MJJA precipitation rate derived from the ERIK run (**a–c**) and control run (**g–i**), and the corresponding spectra in the ERIK run (**d–f**) and control run (**j–l**) for the three sub-regions of the EASM: tropical (6°N–20°N, 100°E–120°E) (*left panels*), subtropical (21°N–35°N, 100°E–120°E) (*middle panels*), and extratropical (36°N–50°N, 100°E–120°E) (*right panels*). The statistical significance of the spectral peaks was tested against the red noise spectrum at 95% confidence level

variations beyond the interdecadal time scale. In order to see the periodicity of the forced response, the corresponding power spectra for each region are shown in Fig. 5d–f, respectively. These forced responses are further compared to the results derived from the free (control) run (Fig. 5g–i for 11-year running mean MJJA mean precipitation and Fig. 5j–l for the corresponding power spectra). The free (control) run allows us to examine the model internal variability due to the feedback processes within the coupled climate system. We note that the results from the free run show no significant centennial–millennial variations in all three regions (Fig. 5g–l). The internal variabilities in all three regions have a common significant energy peak on 50–60 year time scale. In addition, in the subtropical and extratropical regions, another peak at about 90 years is also statistically significant (Fig. 5k, l). On the other hand, the behavior of the forced variations differs from the internal mode. The change of behavior depends on latitude.

The most prominent forced response is found in the extratropics (Fig. 5c, f). The 11-year running mean precipitation displays a pronounced peak at the lowest frequency, whereas the interdecadal peak which is dominant in the free run becomes insignificant. This means that the forced extratropical variation is primarily seen on the millennial time scale. The millennial variation is also

evident by direct examination of the time series in Fig. 5c. The summer mean precipitation rate is 2.12 mm/day during the MWP (1100–1200) while 1.98 mm/day during the LIA (1600–1700) (Table 1), implying a decrease from MWP to LIA by about 6.6%. During the same period, the corresponding effective solar radiation decreased by 1.87 W/m^2 (only about 0.14% of the total insolation at the top of the atmosphere) in the model simulation. This result suggests that the millennial variation of the extratropical EASM is of forced and resonant nature, driving primarily by the given effective solar radiation. This millennial variation might be related to a 1,500-year cycle in some proxy records (Bond et al. 1997; Dima and Lohmann 2009), but the cause of this cycle is still unknown.

The forced responses in the subtropical and tropical EA do not show peaks at the lowest frequency (Fig. 5d, e). However, in the subtropical EA, the summer mean precipitation rate is 5.13 mm/day during the MWP (1100–1200), and decreases to 4.99 mm/day during the LIA (1600–1700), and then increases to 5.07 mm/day during the Present Warm Period (PWP) (Table 1). This long-term variation apparently follows the effective solar radiation forcing, suggesting the subtropical variation also affected by the effective solar radiation forcing on the millennial time scale. Note that although the absolute values of decrease in the subtropics is the same as in the extratropics (both are 0.14), the percentage change in the subtropics (2.7%) is much smaller than that (6.6%) in the extratropics. In this sense, subtropical response is weaker than the extratropical response.

Only in the tropical EA, the changes in summer mean precipitation does not follow the millennial variation of the effective solar radiation forcing (Fig. 5a, d). It means that the given amplitude of effective solar forcing variations in the model is too small to alter the ITCZ over the EA sector, i.e., the ITCZ is more stable than the subtropical and extratropical systems in response to the change of the effective solar radiation. However, an upward trend from LIA to the PWP (1920–1990) is notable (Fig. 5a); the precipitation rate increased significantly by about 0.22 mm/day (Table 1), suggesting that the tropical rainfall significantly responds to the modern anthropogenic radiative forcing.

3.2 Centennial variation

To focus on the centennial variation, the 31-year running mean time series were further examined. Figure 6 presents the precipitation rate averaged over the three latitudinal regions in the forced ERIK run along with the time series of various forcing terms to facilitate comparison. Over the past millennium, the effective solar radiation forcing had experienced six periods of significant minimum, which occurred around 1055, 1270, 1450, 1680, 1820, and 1900, and are superposed on a background of millennial variation. These minima along with the corresponding maxima in between them represent a major portion of the centennial variation in the effective solar radiation forcing. The six minima in the effective solar radiation forcing can be attributed to a combination of the enhanced volcanic activity and decreased solar radiation.

It is of interest to observe that the subtropical (Fig. 6f) and extratropical (Fig. 6g) precipitation intensities tend to reach a minimum following the minimum effective solar radiation forcing. This suggests that both the extratropical and subtropical EA rainfall respond to centennial variation of the effective solar radiation forcing significantly, while the tropical ITCZ does not seem to respond the weakening effective solar radiation periods. On the other hand, the tropical precipitation appears to respond to the increased greenhouse gases forcing. Table 2 shows that in spite of reduction of the degree of freedoms due to smoothing, based on the estimated degree of freedom (Livezey and Chen 1983), significant correlations exist between CO_2 concentration and the tropical EA rainfall and between the effective solar radiation forcing and the subtropical rainfall, respectively. Note that the correlation coefficients in Table 2 reflect correlations on both the centennial and millennial time scales. The good correlation between the CO_2 concentration and the tropical EA rainfall occurs primarily on millennial time scale, while the significant correlation between the effective solar radiation forcing and subtropical EA rainfall occurs primarily on the centennial time scale. The correlation between the effective solar radiation forcing and extratropical EA rainfall occurs in both the millennial and centennial time scales.

4 Meridional structure of the forced mode of the EASM

Due to the large meridional extent of the EASM, an interesting question is how the variations of the tropical, subtropical and extratropical monsoon rainfall are related to each other on millennial time scale. For this purpose, we examine the differences in the horizontal structure between the MWP and LIA epochs (MWP minus LIA), because these two epochs represent two extreme phases of the last millennial variations in effective solar radiation forcing. We also want to find out the structural differences between the external mode (millennial variation) and internal mode (interannual–decadal variation). Note that, the "millennial variation" cannot be regarded as pure externally forced, similarly, the interannual–decadal variation cannot be regarded as purely induced by internal feedback. Therefore, use of external (internal) mode here means that the

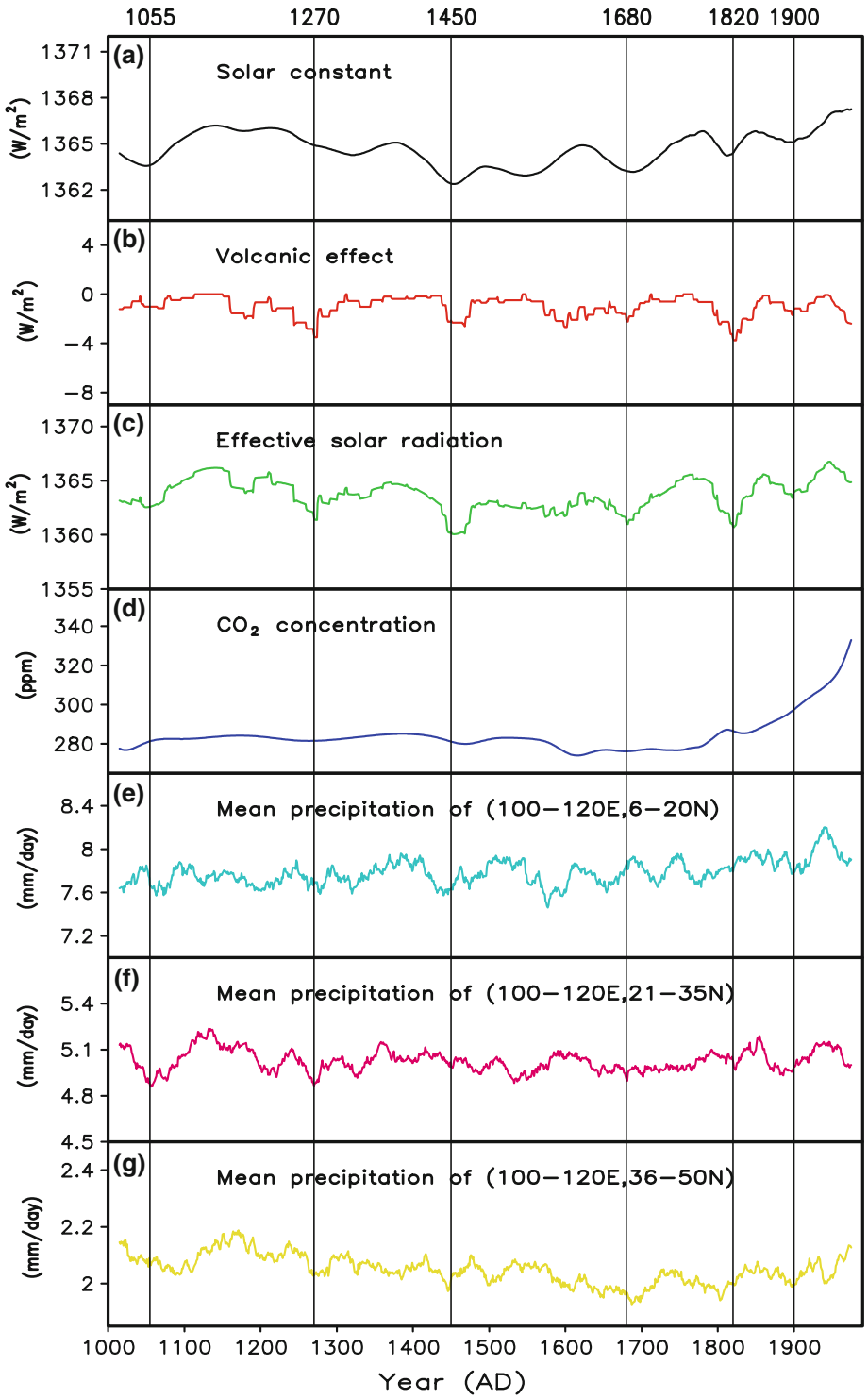

Fig. 6 The 31-year running mean time series of the forcing factors (solar constant (**a**), volcanic aerosol effect (**b**), effective solar radiation forcing (**c**) and CO_2 concentration (**d**)) and the MJJA precipitation rate in the tropics (**e**), subtropics (**f**), and extratropics (**g**)

process that governs the variability is primarily due to external forcing (internal feedback). To derive the structure of the internal mode, we make a composite difference between 'wet' and 'dry' Meiyu years based on the result from ERIK run, because the structures of interannual variations in the free and forced runs have no statistically significant difference. The wet and dry Meiyu years were selected when the Meiyu rainfall in the region (21°N–35°N, 100°E–120°E) is above or below one standard deviation, respectively.

Figure 7 compares the spatial structures of the forced mode (Fig. 7a) and internal mode (Fig. 7b). With regard to the relationship between the subtropical and extratropical rainfall, there is a difference between the forced and

Table 2 Correlation coefficients between the three regional precipitation intensity indices and the effective solar radiation forcing and CO_2 concentration over the past millennium

Correlation coefficient	Effective solar radiation	CO_2 concentration
Tropical rainfall (6°N–20°N, 100°E–120°E)	0.34	0.51**
Subtropical rainfall (21°N–35°N, 100°E–120°E)	0.46*	0.23
Extratropical rainfall (36°N–50°N, 100°E–120°E)	0.37	0.19

The coefficient was calculated by using 31-year running mean time series

* Represent statistically significant at 95% confidence level

** Represent statistically significant at 99% confidence level

internal modes. For the forced mode, the subtropical and extratropical rainfall increases simultaneously (Fig. 7a). This feature implies that the forced mode is characterized by an in-phase relationship between the subtropical and extratropical rainfall. On the other hand, the internal mode features an out-of-phase relationship between the subtropics and extratropics (Fig. 7b). Note that the model simulated internal mode structure agrees well with the observed structure on interannual–decadal time scale: When Meiyu is abundant, the rainfall in northern China tends to be deficient or vice versa (e.g., Ding 1992).

As far as the tropical–subtropical rainfall relationship is concerned, the two modes have similar structures, i.e., the tropical monsoon rainfall tends to weaken when the subtropical monsoon enhances (Fig. 7a, b), suggesting an anti-correlation between the tropical (ITCZ) and subtropical (Meiyu) rainfall. Therefore, under the moderate radiative forcing change on the millennial time scale (such as that in the ERIK run), the ITCZ and Meiyu rainfall remains anti-correlated (Fig. 7a), which is similar to that of the internal mode (Fig. 7b). Why is the Meiyu–ITCZ relationship similar in the forced and internal modes? Because the wet–dry contrast of the interannual–decadal variation is primarily determined by ENSO variation in the model. The structure of the interannual variation shown in Fig. 7b is essentially the same as in modern observation (e.g., Ding 1992). The ENSO-induced Philippine Sea anticyclonic anomaly is a key system, which suppress ITCZ while enhances Meiyu, forming the anti-correlation between tropics and subtropics (Wang et al. 2000).

The spatial structure of the forced response can be understood in terms of traditional thinking of the effects of land–sea thermal contrast. When the effective solar radiation forcing increases, as indicated by the MWP minus LIA difference, the surface air temperature increases over the East Asian continent, especially in the mid-latitude, more rapidly than over the adjacent ocean (Fig. 8). Due to the different thermal capacity of the land and ocean, the resulting land–ocean differential warming amplifies the pressure gradient between the land and ocean. For instance, the 850 hPa geopotential height over the Lake Baikal and western central China is 4–5 m lower than those over the northwestern Pacific and the northern South China Sea–Philippine Sea (Fig. 8). Corresponding to this pressure change, southwesterly is enhanced over southern China and southerly winds extend from the Yangtze River Valley (30°N) to northern China (50°N) (Fig. 8). Therefore, the rainfall increases in both southern and northern China, while suppressed in the South China Sea–Philippine Sea (Fig. 7a).

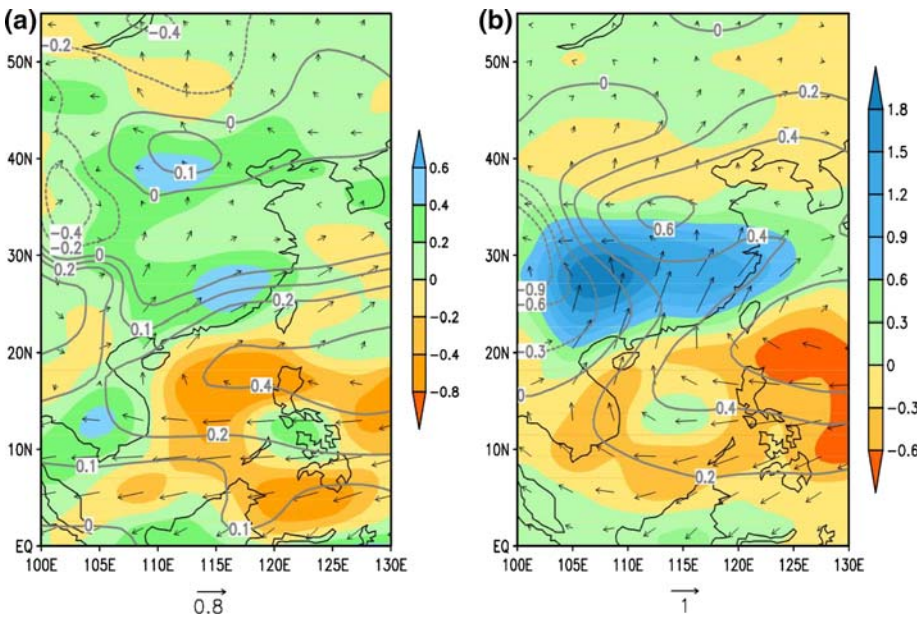

Fig. 7 Comparison of the spatial structures of the (**a**) forced and (**b**) internal mode. The structure of the forced mode is described by the differences between the MWP and LIA (MWP minus LIA). The structure of the internal mode is depicted by the composite strong minus weak subtropical (21°N–35°N, 100°E–120°E) rainfall of the interannual–decadal variation. The *color shading* represents the MJJA mean precipitation rate (mm/day), *contours* denote the sea-level pressure (hPa), and *arrows* represent the 850 hPa winds (m/s)

The structural difference between the internal and forced EASM modes in the extratropics is consistent with the latitudinal dependence of the forced response. The change of the subtropical–extratropical monsoon relationship in the forced mode is due to the sensitive response of the extratropical monsoon. The latitudinal dependence of the response is arguably arising from the latitudinal differential warming in response to the increased effective solar radiation forcing during the MWP, i.e., the degree of warming in high-latitudes is much larger than the slight tropical warming. As a result, the sea-level pressure drops significantly in high latitude and northern central China (Figs. 7a, 8), inducing southerly increases across the subtropical and extratropical monsoon regions.

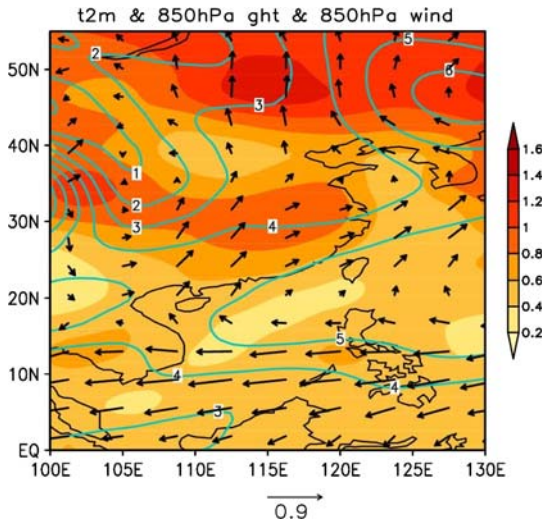

Fig. 8 The differences between MWP and LIA (MWP minus LIA) in the MJJA mean surface air temperature (*shading* in unit of K), 850 hPa geopotential height (*solid contours* in unit of m) and 850 hPa wind (*vector* in unit of m/s)

5 Modulation of the internal mode by the external forcing

It is seen, from the previous section, that the summer mean states averaged over a 100-year period show significant differences between the MWP and LIA epochs over the midlatitude EA. Would this change in the climatological mean state affect the interannual variations, or the behavior of the internal mode? To address this question, an empirical orthogonal function (EOF) analysis of the combined precipitation and 850 hPa winds was applied to the two epochs separately. For each epoch, the dominant EOF mode is statistically distinguished from all rest of the EOF modes based on the significant test proposed by North et al. (1982). The fractional variance explained by the EOF1 of MWP and LIA is 32.5 and 32.8%, respectively. Therefore, a comparison of the leading EOF modes for the two epochs was made.

Figure 9 shows the spatial pattern of the leading EOFs of the interannual variation of the EASM and the spectrum of the corresponding principal component for the MWP

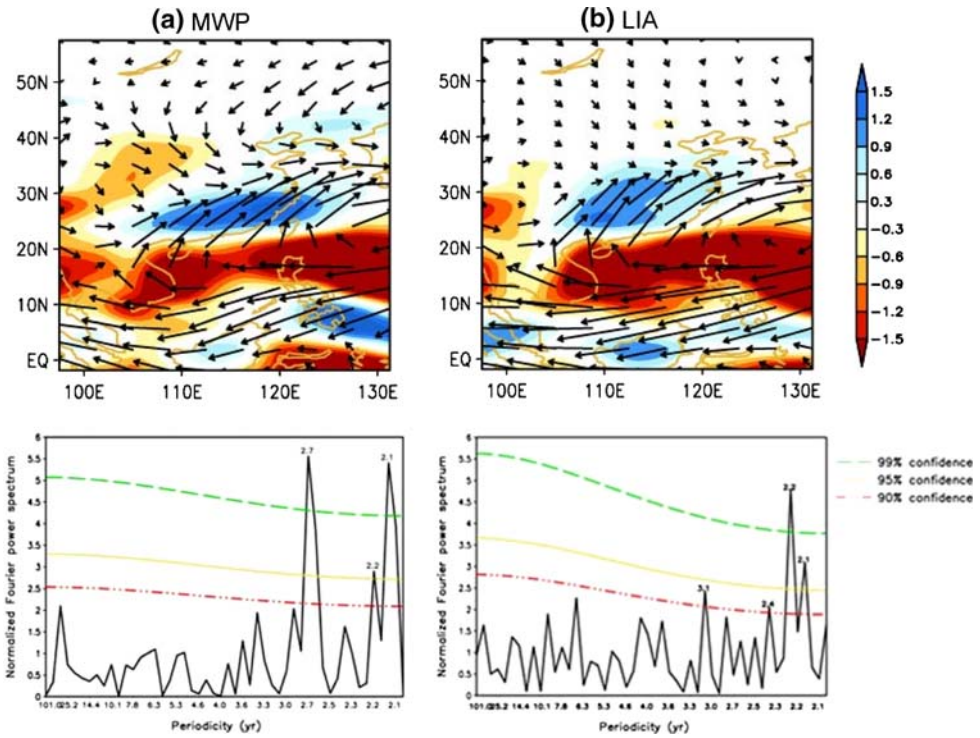

Fig. 9 The spatial structure (*upper panel*) and spectrum of the corresponding principal component (*lower panels*) of the leading empirical orthogonal functions of the precipitation and 850 hPa winds derived for the period of (**a**) MWP and (**b**) LIA epochs. The data were derived from the forced ERIK run

and LIA epoch. It can be seen that the two leading EOFs show similar spatial patterns over the tropics and subtropics, i.e., an elongated, enhanced Subtropical High dominates the northern South China Sea and northern Philippine Sea with suppressed precipitation along the ridge of the Subtropical High and enhanced rainfall along the northwest flank of the Subtropical High (namely enhanced Meiyu). This anomalous pattern is quite similar to the leading EOF mode of the interannual variation of the EASM derived from the modern observations (e.g., Wang et al. 2008). This similarity suggests that over the tropics and subtropics, the leading internal mode does not have significant difference between the MWP and LIA. This is consistent with the finding that the millennial variation of the EASM in response to the effective solar radiation forcing is negligibly small in the tropics and moderate in the subtropics.

On the other hand, since the millennial variation of the EASM over the midlatitude has considerable amplitude (Figs. 7a, 8), one would anticipate this change might have an impact on the behavior of the internal mode over the midlatitude. Indeed, as shown in Fig. 9a and b, there are evident differences on precipitation and winds between the two epochs over the latitudes north of 35°N. A prominent cyclonic anomaly dominates the entire extratropical EA during the MWP epoch with enhanced precipitation anomalies accompanying this cyclonic circulation anomaly. However, these extratropical anomalies were absent during the LIA period. This result suggests that during the warm epoch (MWP), the interannual variation of the summer monsoon over the midlatitude of EA is actively coupled with the tropical–subtropical variation due to excessive warming of the midlatitude continent. On the other hand, during the cooling epoch (LIA), the interannual variability of the summer monsoon over the midlatitude is inactive or not in connection with the variation in the tropics and subtropics. In accordance with this change of spatial anomaly pattern (or coupling between the midlatitude and tropics) the periodicity of the temporal variation of the leading EOF also shifts to a lower frequency: In the MWP, a new peak on 2.7 year becomes a pronounced compared to that in the LIA epoch (Fig. 9a, b).

6 Concluding remarks

Over the last millennium, the effective solar radiation has experienced an appreciable variation. However, the amplitude of the forcing estimated from proxy data has uncertainties. In the ECHO-G forced simulation, the differential effective solar radiation forcing has assumed a magnitude of about 2 W/m^2 between the MWP and LIA. Given this moderate millennial variation in the external forcing, the simulated surface air temperature variation over China compares favorably with that deduced from multiple sources of proxy evidences (Fig. 4). The model also reproduces reasonably realistic present-day climatology of the EASM, including both the long-term mean and the annual cycle (Figs. 2, 3). Thus, the model performance adds confidence to our analysis of precipitation variability on interannual to millennial time scales.

One of the major findings of this study is that the climate response of EASM to the external radiative forcing depends on latitude (Fig. 5). On the millennial time scale, (a) The intensity of the extratropical precipitation follows the millennial variation in the effective solar radiation forcing most closely, while the intensity of the tropical precipitation follows the millennial variations of the CO_2 concentration most closely; (2) the subtropical precipitation (or Meiyu) responds to the millennial forcing less sensitively than the midlatitude, but the differences between the MWP and LIA remain significant (Table 1); (3) the tropical East Asia (ITCZ), however, has no appreciable response to the given millennial effective solar radiation forcing, suggesting that the ITCZ is more stable and hard to be perturbed. On the other hand, the precipitation in the ITCZ responds to the CO_2 concentration more sensitively than the subtropical and extratropical EA rainfall (Table 1). On the centennial time scale, there were six significant minimum values in the effective solar radiation forcing (Fig. 6), which are attributed to a combined variation of the enhanced volcanic activity and decreased solar radiation at the top of the atmosphere. It is found that both the extratropical and subtropical EA rainfall intensities tend to be weak when the effective solar radiation forcing is relatively low (Fig. 6).

It is also found that the forced mode has a different structure in comparison to the internal mode of EASM in the extratropical regions. As shown by the modern meteorological record and in the model (Fig. 7b), for the internal mode, an abundant subtropical rainfall corresponds to a deficient extratropical rainfall. In the forced response, however, the extratropical and subtropical monsoons vary in tandem (Fig. 7a). On the other hand, because the tropical monsoon is insensitive to the millennial change in the effective solar radiation forcing, the relationship between the ITCZ and Meiyu remains anti-correlated for the forced mode, which is similar to the interannual variations (Fig. 7a, b).

Another interesting finding from this model study is that the behavior of the internal mode (the interannual–decadal variation) is modulated by change of the mean states on the millennial time scale (Fig. 9). The inference is that when the external forcing increases, the behavior of the interannual variability might change accordingly, especially in the extratropics.

The results obtained from this model studies have important ramifications. First, the latitudinal dependence of the monsoon response implies that the proxy evidences collected in the relatively dry, extratropical EA may more sensitively reflect the forced variability in the historical records. This assertion is, to some degree, supported by the proxy evidence found at Wanxiang cave by Zhang et al. (2008). The Wanxiang Cave (33°19′N, 105°00′E, 1,200 m above sea level) is located in between the Qinghai-Tibetan Plateau and the Chinese Loess Plateau in Wudu County, Gansu Province (Fig. 10a). Based on the annual precipitation distribution, the Wanxiang cave is located north of the subtropical Meiyu zone and may represent extratropical dry climate regime (note that the actual climate regime depends not only latitude but also the distance from the adjacent ocean, see Fig. 10a). Figure 10c indicates that the simulated time series surrounding the Wanxiang Cave (31°N–35°N, 100°E–110°E, blue rectangle in Fig. 10a) is similar to the model extratropical time series (correlation coefficient: 0.69). This suggests that Wanxiang cave variability indeed belongs to the extratropical "regime". It is anticipated, from the present model analysis, that the rainfall response to millennial radiative forcing variation at that place should be sensitive. It was suggested that the calcite was deposited in isotopic equilibrium and that the δ^{18}O signal in this cave largely anti-correlates with precipitation (Zhang et al. 2008). Figure 10b shows that the model simulated millennial rainfall variation near the Wanxiang Cave indeed compares favorably with the rainfall deduced from the δ^{18}O series at Wanxiang Cave with a correlation coefficient of −0.49. This agreement, however, is mainly due to the variation on the millennial time scale; on the centennial time scale (100–200 years), the model result and cave record do not match. What causes this mismatch needs further exploration.

Second, the different meridional structures between the forced and internal modes mean that the same EASM index may have different meanings on the interannual and millennial time scales. On the millennial time scale, a strong EASM can be measured consistently by both the

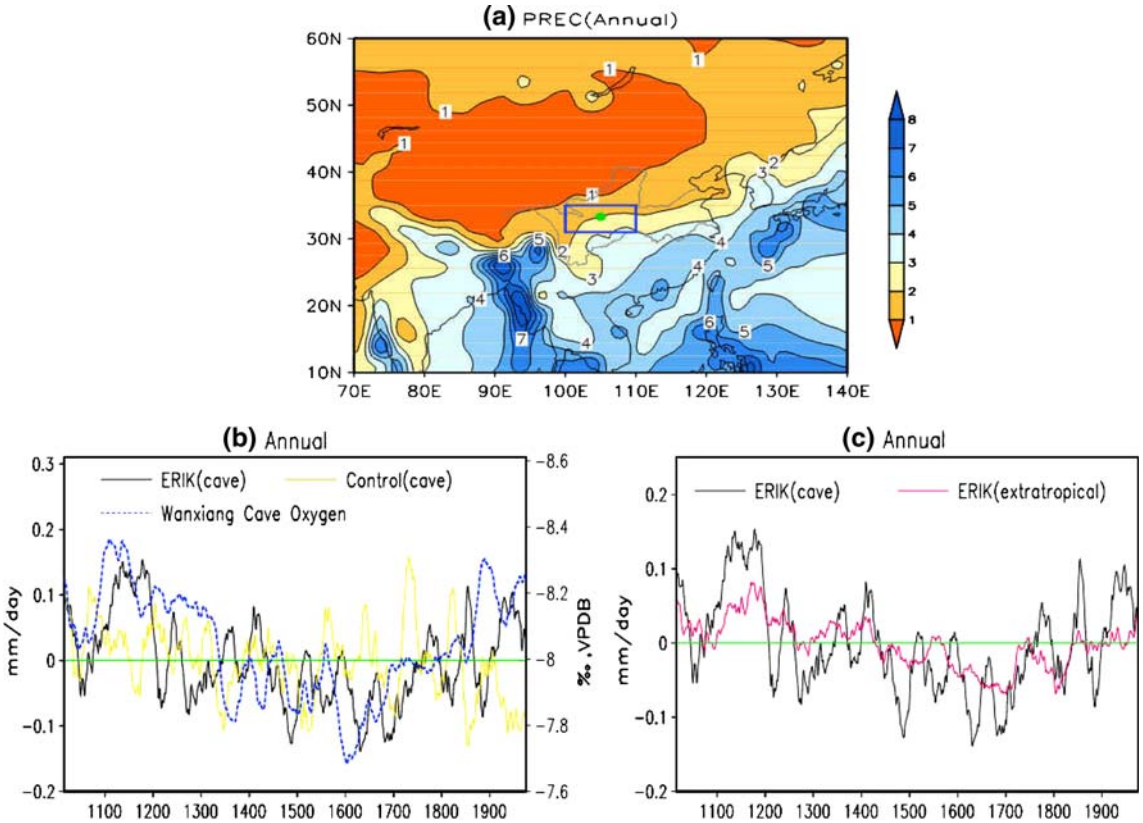

Fig. 10 **a** The location of the Wanxiang Cave (33°19′N, 105°00′E, *green circle*) and the climatological mean MJJA precipitation rate derived from the observed (PREC) data for the period of 1961–1990 (Contours with interval 1 mm/day). **b** Comparison of the 31-year running means of the δ^{18}O series from Wanxiang Cave (note that the sign has been reversed to facilitate comparison; the data were adopted from Zhang et al. (2008)) and the simulated rainfall (mm/day) averaged in the region surrounding the Wanxiang cave (31°N–35°N, 100°E–110°E: the *blue rectangle*) from the ERIK run and control run. **c** Comparison of the 31-year running means of the simulated rainfall (mm/day) averaged in the region surrounding the Wanxiang cave and averaged in the extratropics (36°N–50°N, 100°E–120°E) from the ERIK run

subtropical and extratropical rainfall; thus, use of the northern China rainfall (or penetration of southerly to northern China) as a measure of EASM strength is appropriate. This is in sharp contrast to the internal mode, where an abundant northern China rainfall means a deficient Meiyu and thus use northern China rainfall as a measure is inconsistent with the Meiyu variability in modern meteorology. Since the Meiyu is a major precipitation agent in EA, calling a weak Meiyu as a strong EASM is at odds with the convention by which a strong monsoon is defined, for instance in India.

While the relationship between the ITCZ and Meiyu remains anti-correlated on the millennial time scale, it is anticipated that when the external forcing is sufficiently strong such as the case on the orbital time scale, the impact of the external forcing might penetrate to the tropics, thereby changing the ITCZ–Meiyu relationship. To test this hypothesis, analysis of the PMIP-III multi-model simulation may provide physical insight.

Direct comparison of the model simulation with proxy data remains a challenge. The favorable agreement between the simulation and proxy data as presented in Figs. 4 and 10b is qualitative. The magnitude of the millennial variation of the effective solar forcing has certain degree of uncertainties. If the amplitude of the effective solar radiation forcing reduces, the response is expected to be smaller but it would not be in a linear fashion. In order to make a convincing model-data comparison, all sources of uncertainty should be taken into account, including the uncertainties in the model effective solar radiation, the model physics and the proxy data. The implication is that (a) multi-model intercomparison is needed to reduce the model uncertainties; (b) multi-source proxy data should be constructed to reduce the proxy data uncertainty; and (c) different strength of forcing should also be used in multi-model framework to assess the impact of the uncertainty in external forcing.

Acknowledgments We acknowledge the financial supports from the National Basic Research Program of China (Grant Nos. 2004CB720208 and 2010CB833406), the Innovation Project of Chinese Academy of Sciences (Grant Nos. KZCX2-YW-315, KZCX2-YW-319 and KZCX2-YW-337), and the Natural Science Foundation of China (Grant Nos. 40890054, 40871007 and 40672210). We also thank Drs. Eduardo Zorita, Bao Yang and Pingzhong Zhang for providing their corresponding data for this study.

References

Blunier T, Chappellaz JA, Schwander J et al (1995) Variations in atmospheric methane concentration during the Holocene epoch. Nature 374:46–49

Bond G, Showers W, Cheseby M, Lotti R, Almasi P, deMenocal P, Priore P, Cullen H, Hajdas I, Bonani G (1997) A pervasive millennial-scale cycle in North Atlantic Holocene and glacial climate. Science 278:1257–1266

Chang CP, Zhang Y, Li T (2000a) Interannual and interdecadal variations of the East Asian summer monsoon and tropical Pacific SSTs. Part I. Roles of the subtropical ridge. J Clim 13:4310–4325

Chang CP, Zhang Y, Li T (2000b) Interannual and interdecadal variations of the East Asian summer monsoon and tropical Pacific SSTs. Part II. Meridional structure of the monsoon. J Clim 13:4326–4340

Crowley TJ (2000) Causes of climate change over the past 1000 years. Science 289:270–277

Dima M, Lohmann G (2009) Conceptual model for millennial climate variability: a possible combined solar-thermohaline circulation origin for the ~1,500-year cycle. Clim Dyn. doi:10.1007/s00382-008-0471-x

Ding YH (1992) Summer monsoon rainfalls in China. J Meteorol Soc Jpn 70(1B):373–396

Ding YH, Sikka DR (2006) Synoptic systems and weather. In: Wang B (ed) The Asian monsoon. Springer, New York, pp 131–201

Etheridge D, Steele LP, Langenfelds RL et al (1996) Morgan natural and anthropogenic changes in atmospheric CO_2 over the last 1000 years from air in Antarctic ice and firn. J Geophys Res 101:4115–4128

Fu CB (1987) El Niño/South oscillation phenomenon and interannual climate variations. Sci Atmos Sin 11(2):209–219 in Chinese

Guo QY (1983) The summer monsoon index in East Asia and its variation. Acta Geogr Sin 38:208–217 in Chinese

Huang RH, Wu Y (1989) The influence of ENSO on the summer climate change in China and its mechanisms. Adv Atmos Sci 6:21–32

Ju J, Slingo JM (1995) The Asian summer monsoon and ENSO. Quart J Roy Meteorol Soc 121:1133–1168

Kanamitsu M, Ebisuzaki W, Woollen J, Yang SK, Hnilo JJ, Fiorino M, Potter GL (2002) NCEP-DOE AMIP-II reanalysis (R-2). Bull Am Meteorol Soc 83:1631–1643

Kang I-S, Jin K, Wang B, Lau K-M, Shukla J, Krishnamurthy V, Schubert SD, Wailser DE, Stern WF, Kitoh A, Meehl GA, Kanamitsu M, Galin VY, Satyan V, Park C-K, Liu Y (2002) Intercomparison of the climatological variations of Asian summer monsoon precipitation simulated by 10 GCMs. Clim Dyn 19:383–395

Lau N-C, Nath MJ (2000) Impact of ENSO on the variability of the Asian-Australian monsoons as simulated in GCM experiments. J Clim 13:4287–4309

Lau N-C, Nath MJ (2006) ENSO modulation of the interannual and intraseasonal variability of the East Asian Monsoon—a model study. J Clim 19(18):4508–4530

Legutke S, Voss R (1999) The Hamburg atmosphere–ocean coupled circulation model ECHO-G. Technical report no. 18, German Climate Computer Center (DKRZ), pp. 61

Liu J, Wang B, Yang J (2008) Forced and internal modes of variability of the East Asian summer monsoon. Climate of the Past 4:225–233

Livezey RE, Chen WY (1983) Statistical field significance and its determination by Monte Carlo techniques. Mon Weather Rev 111:46–59

Matsumoto J, Murakami T (2002) Seasonal migration of monsoons between the northern and southern hemisphere as revealed from equatorially symmetric and asymmetric OLR data. J Meteorol Soc Jpn 80:419–437

Nitta T (1987) Convective activities in the tropical western Pacific and their impact on the Northern-Hemisphere summer circulation. J Meteorol Soc Jpn 65:373–390

North GR, Bell TL, Cahalan RF, Moeng FJ (1982) Sampling errors in the estimation of empirical orthogonal functions. Mon Weather Rev 110(7):699–706M

Robock A, Free M (1996) The volcanic record in ice cores for the past 2000 years. In: Jones P, Bradley R, Jouzel J (eds) Climatic variation and forcing mechanisms of the last 2000 years. Springer, New York, pp 533–546

Roeckner E, Arpe K, Bengtsson L, Christoph M, Claussen M, Dumenil L, Esch M, Giorgetta M, Schlese U, Schulzweida U (1996) The atmospheric general circulation model ECHAM4: model description and simulation of present-day climate. MPI report no. 218. Max-Planck-Institut f̈ur Meteorologie, Hamburg, pp. 90

Tao SY, Chen L (1987) A review of recent research on East Asian summer monsoon in China. In: Chang CP, Krishnamurti TN (eds) Monsoon meteorology. Oxford University Press, London, pp 60–92

Wang B, LinHo (2002) Rainy season of the Asian–Pacific summer monsoon, J Clim 15(4):386–398

Wang B, Zhang Q (2002) Pacific–East Asian teleconnection. Part II. How the Philippine Sea anomalous anticyclone is established during El Niño development. J Clim 15:3252–3265

Wang B, Wu R, Fu X (2000) Pacific-East Asia teleconnection: how does ENSO affect East Asian climate? J Clim 13:1517–1536

Wang B, Kang I, Lee J (2004) Ensemble simulations of Asian–Australian monsoon variability by 11 AGCMs. J Clim 17:803–818

Wang YJ, Cheng H, Edwards RL, He YQ, Kong XG, An ZS, Wu JY, Kelly MJ, Dykoski CA, Li XD (2005) The Holocene Asian monsoon: links to solar changes and North Atlantic climate. Science 308:854–857

Wang B, Wu Z, Li J, Liu J, Chang CP, Ding Y, Wu G (2008) How to measure the strength of the East Asian summer monsoon? J Clim 21:4449–4463

Wolff J-O, Maier-Reimer E, Legutke S (1997) The Hamburg ocean primitive equation model. Technical report no. 13, German Climate Computer Center (DKRZ), Hamburg, pp. 98

Xie P, Arkin PA (1995) An intercomparison of gauge observations and satellite estimates of monthly precipitation. J Appl Meteorol 34:1143–1160

Yancheva G, Nowaczyk NR, Mingram J, Dulski P, Schettler G, Negendank JFW, Liu J, Sigman DM, Peterson LC, Haug GH (2007) Influence of the intertropical convergence zone on the East Asian monsoon. Nature 445:74–77

Yang B, Braeuning A, Johnson KR (2002) General characteristics of temperature variation in China during the last two millennia. Geophys Res Lett 29(9). doi:10.1029/2001GL014485

Zhang PZ, Cheng H, Edwards RL, Chen F, Wang Y, Yang X, Liu J, Tan M, Wang X, Liu J, An C, Dai Z, Zhou J, Zhang D, Jia J, Jin L, Johnson KR (2008) A test of climate, sun, and culture relationships from an 1810-year Chinese cave record. Science 322:940–942

Zorita E, Gonzalez-Rouco JF, Legutke S (2003) Testing the Mann et al (1998) approach to paleoclimate reconstructions in the context of a 1000-yr control simulation with the ECHO-G coupled climate model. J Clim 16:1378–1390

Zorita E, Gonzalez-Rouco JF, von Storch H, Montavez JP, Valero F (2005) Natural and anthropogenic modes of surface temperature variations in the last thousand years. Geophys Res Lett 32:L08707. doi:10.1029/2004GL021563